Physics – Uspekhi **48** (11) 1151 – 1159 (2005)

INSTRUMENTS AND METHODS OF INVESTIGATION PACS numbers: **07.57.–c**, 42.27.Te, **68.03.–g**

Water surface structures observed using infrared imaging

G R Ivanitskii, A A Deev, E P Khizhnyak

DOI: 10.1070/PU2005v048n11ABEH004685

Contents

Abstract. **Modern infrared focal plant array cameras with thermal sensitivities up to 0.01 – 0.02 °C have made it possible to form a novel view of various physical, chemical, and biological processes that involve both the heat production and mobility of fluids affected by local thermal gradients. The mobility of water is important, especially in studying the formation mechanisms of water structures due to Rayleigh – Bénard convection. Various water structures can successfully be studied using infrared imaging.**

1. Introduction

Infrared (IR) radiation in the wavelength ranges 3 – 5 μm and 8 – 12 μm is weakly absorbed and scattered in air. This makes it possible to record the spatiotemporal distribution of temperature in various physical and biological phenomena.

2. Modern infrared-imaging equipment

Two or three decades ago, IR imaging was mainly intended for military applications. Nowadays, it has become an information technology with an extended area of use. Optical – mechanical image scanning is not employed in the third generation of IR imagers, which therefore have high operation speeds and relatively small masses, sizes, and energy consumption; in addition, they produce no noise and ensure high signal-to-noise ratios. Modern IR cameras are characterized by high image quality and can be coupled with computers, which permits real-time digital image processing.

The most widespread third-generation IR cameras have thermal sensitivities up to 0.02 °C, time resolutions 100 – 200 frames per second, spatial resolutions $(3-5)\times10^{-5}$ m, and matrices of 320 × 240 pixels. They allow forming a novel view of the heat-production processes, mobility of substances under the action of local thermal gradients, and information processes of detecting, recognizing, and classifying heat-emitting objects. IR radiation is emitted due to oscillations of atoms, rather than electrons, within molecules; for this reason, remote IR spectroscopy with identification of molecules can in some cases be implemented based on such measurements.

About 20 companies in the US, France, Sweden, Japan, China, and Russia produce third-generation IR imagers. The best samples have already reached the thermal resolution 0.01 °C, spatial resolution 640 × 512 pixels, and temporal resolution up to 8000 frames per second. Cameras with matrices having up to 960 × 1280 pixels, amplitude resolutions up to 0.001 °C, and the same time parameters are forthcoming on the market. Modern IR imagers are cooled thermoelectrically and do not require special cooling agents.

Planar IR-photodetector matrices can be made of various materials, such as lead chalcogenides, cadmium – mercury – tellurium compounds, indium antimonide, platinum silicide, impurity silicon and germanium, or multilayered structures with quantum wells (so-called quantum-well infrared photodetectors, QWIPs). The theoretical foundations of the development of IR-imaging equipment are considered in Refs [1 – 5].

IR imaging is not only measuring the temperature relief of the surface of an object. 'Imaging' is the key component of the term *IR imaging*. Specifically, *IR imaging* is an information process that allows viewing the object as a whole, isolating heat sources on and inside it, and identifying, recognizing, and classifying their essential features.

In our experiments, we used IR-imaging systems with indium – antimonide matrices, whose thermal sensitivity at the recording rate 150 frames per second is no worse than

G R Ivanitskii, A A Deev Institute of Theoretical and Experimental Biophysics, Russian Academy of Sciences,
Institutskaya ul. 3, 142290 Pushchino, Moscow Region,
Russian Federation
Tel. (7-0967) 73 24 81. Fax (7-0967) 79 05 53
E-mail: ivanitsky@iteb.ru, deev@iteb.ru
E P Khizhnyak Institute of Cell Biophysics, Russian Academy of Sciences,
Institutskaya ul. 3, 142290 Pushchino, Moscow Region,
Russian Federation
Tel. (7-0967) 73 24 81. Fax: (7-0967) 79 05 53
E-mail: eugene@iteb.ru

Received 29 March 2005, revised 26 July 2005
Uspekhi Fizicheskikh Nauk **175** (11) 1207 – 1216 (2005)
Translated by A V Getling; edited by A M Semikhatov

0.02 °C in the wavelength range 3 – 5 μm and 0.04 °C in the wavelength range 8 – 12 μm and which have the spatial resolution 320 × 240 pixels per frame; thus, in view of the action of the optical system, events can be recorded at an absolute spatial resolution no worse than 30 μm. The thermal sensitivity can be increased to 0.01 – 0.005 °C by means of signal accumulation, if the number of frames is reduced. As is known, the thermal sensitivity increases proportionally to $t^{1/2}$, where t is the signal-accumulation time.

Our three illustrations demonstrate the potentialities of third-generation IR imagers. Figure 1 shows the brickwork of a wall, distinguishable in the IR image even through a 3-cm-thick plaster layer [6]. Figure 2 is an example of medical diagnostics [7 – 9]. The example in Fig. 3 demonstrates the spatial resolution of the instrument. The outlet of a single pore canaliculus, about 30 μm across, can be distinguished on the human body. The dark dots on the fingers are sweat pores.

We here describe the observation of water surface structures by an IR imager. Because water is the basic substance of every living thing and the surface of a living organism is covered with a moisture film, we found it interesting to observe, using IR imaging, macroscopic thermal structures that form in water as it is cooled within the physiological range of temperatures, 20 – 40 °C.

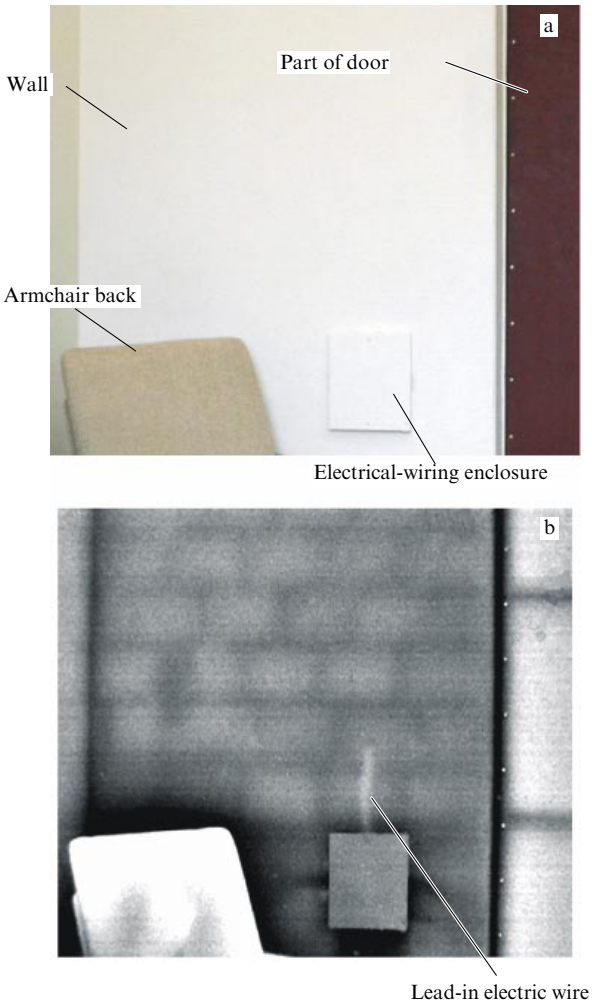

Figure 1. Detection of the brickwork of a wall through a plaster layer: (a) visible-light image of the wall; (b) IR image of the wall.

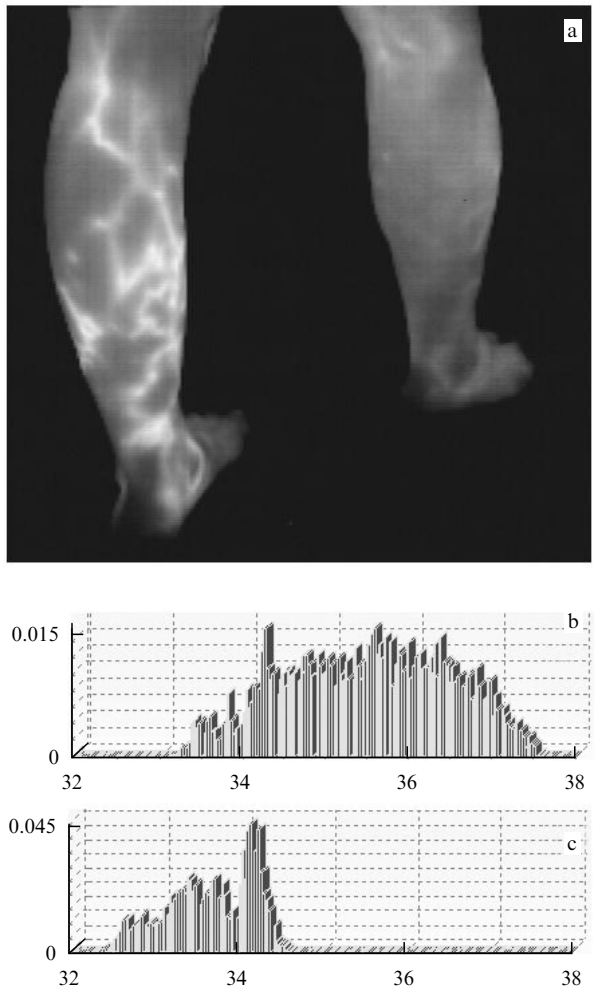

Figure 2. Example of IR-imaging diagnostics of varicose veins in the left leg: (a) thermal portrait of the legs of an afflicted man; (b, c) normalized histograms of temperature distribution over the left and right legs, respectively. Abscissas: temperature in degrees centigrade; ordinates: normalized histogram values in fractions of the total histogram area (set equal to unity).

3. Cellular water-convection macrostructures

Figure 4a shows water cells recorded by us, using IR instrumentation, in the range 8 – 12 μm. They are virtually indistinguishable to the naked eye in visible light. Temperature profiles along various directions in the bulk of the water are shown in Figs 4b – 4e. The thermal gradients result in the development of a cellular pattern in water.

Until recently, the most widespread visualization technique was the so-called *shadowgraph method* [10], which uses the temperature dependence of the light-refraction index. Cold downflows focus light and appear bright as projected onto a screen, while warm upflows, which scatter light, appear dark. The shadowgraph method has a relatively low resolution, however. To visualize flows, experimenters also used special additions (of powder or dye) [11], the Doppler effect in the laser-illuminated sample [12], and optical interferometry [13]. IR imaging permits not only observing water structures indistinguishable to the eye but also recording the dynamics of their evolution.

We do not dwell on the mathematical description of these processes here, because a review article on this subject has already been published in *Physics – Uspekhi* [10].

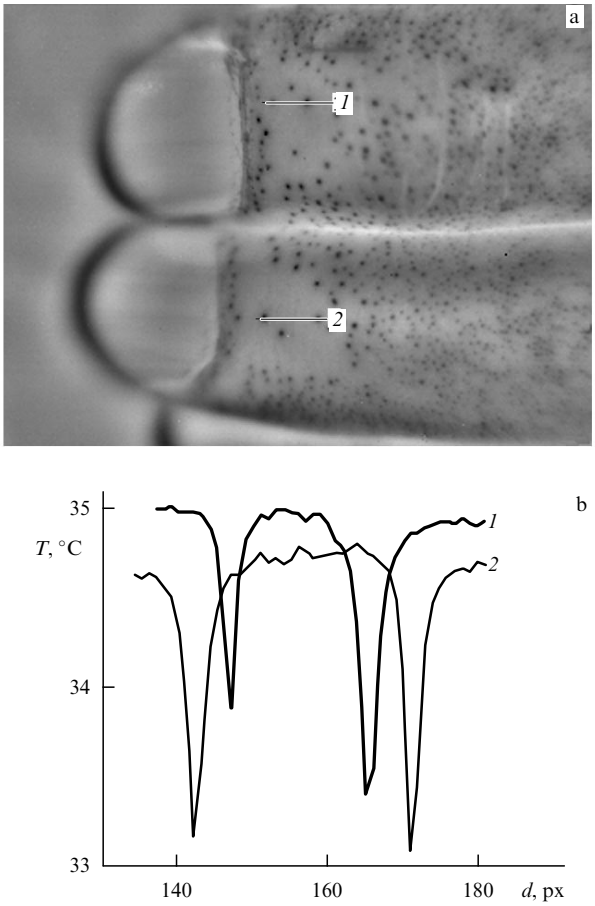

Figure 3. Thermographic visualization of the outlets of sweat-gland canaliculi on the surface of the hand. The thermal resolution is 20 mK and the spatial resolution reaches 30 μm. (a) Thermal portrait of the fingers with sweat canaliculi (dark dots). (b) Temperature profiles along lines *1* and *2* on the two fingers shown in Fig. 3a; horizontal coordinate: the distance along lines *1* and *2*, *d*, in pixels (px); 1 mm = 8 px.

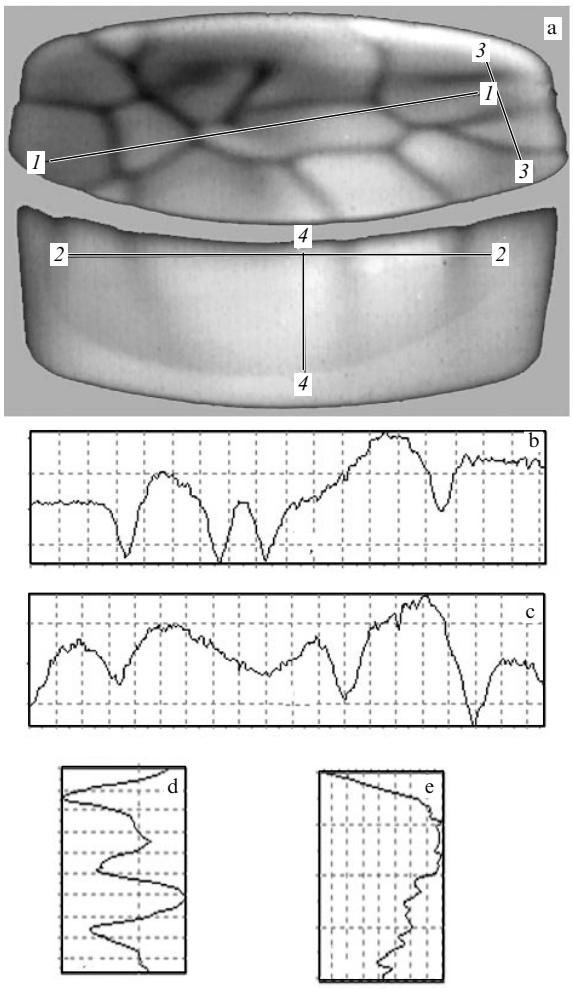

Figure 4. Evaporation-induced water cells as observed in the IR range 8–12 μm in a container of diameter 17 cm. (a) The lines specifying the directions for which the temperature profiles are shown: (b) *1–1*, (c) *2–2*, (d) *3–3*, and (e) *4–4*. The temperature scale is the same for all four profiles — the distance between horizontal dashed lines corresponds to 1 °C along the vertical axis.

Here, we restrict ourselves to only a few notes concerning the mechanisms of cell-pattern formation in water. To evaluate the effect of one parameter or another on the pattern formation in water (or other fluids), a set of dimensionless parameters (the Rayleigh, Prandtl, Marangoni numbers, etc.) is normally used. We recall that the *Rayleigh number* (Ra) characterizes the convective instability due to the depth variation in the fluid density because of the temperature variation. This number depends on the external conditions (the heating intensity) and is proportional to the temperature difference ΔT between fluid layers.

The *Prandtl number* (Pr) is the ratio of the kinematic viscosity of the fluid (ν) to its thermal diffusivity ($\varkappa$). The following example clarifies the physical meaning of the Prandtl number. The oscillation period of the surface fluid layer coincides, to an order of magnitude, with the thermal-diffusion time $h^2/\varkappa$, where h is the vertical scale, i.e., the depth of the fluid layer. At the same time, a low-frequency convective instability occurs, which results in the rearrangement of the entire pattern; its period is h^2/ν. These quantities are different for fluids with different thermal diffusivities and viscosities. For example, the viscosity of water is several orders of magnitude lower than the viscosities of oils (the kinematic viscosity of water is $\nu_{\mathrm{w}} = 1\ \mathrm{cm^2\,s^{-1}}$, while that of a silicone oil, for example, is $\nu = 9000\ \mathrm{cm^2\,s^{-1}}$), and therefore the initiation of low-frequency convection processes in water requires smaller temperature differences between layers than in an oil. Moreover, the viscosities of oils depend strongly on temperature. We recall that the Prandtl number of water varies over the temperature range from 0 °C to 100 °C by a factor of about eight (Pr = 13.5 at $T = 0$ °C and 1.75 at $T = 100$ °C), while the Prandtl number of transformer oil varies over the same temperature range from 43.9 to 866, i.e., by a factor of almost 20. For liquid metals, Pr $\ll 1$, and its temperature dependence is weak (for example, as the temperature varies from 100 °C to 700 °C, the Prandtl number of the alkali metal of sodium varies from 0.0115 to 0.0039, i.e., only threefold). Thus, the Prandtl number characterizes the properties of the fluid itself.

If the Prandtl number is not too small, then, as the stability threshold is passed, thermal convection in a fluid sets in as a steady flow. If the Rayleigh number exceeds its critical value, two or more longitudinal and transverse modes can be excited. The former correspond to convection along the axis of the container and the latter to transverse oscillations on the surface, in the plane normal to the axis.

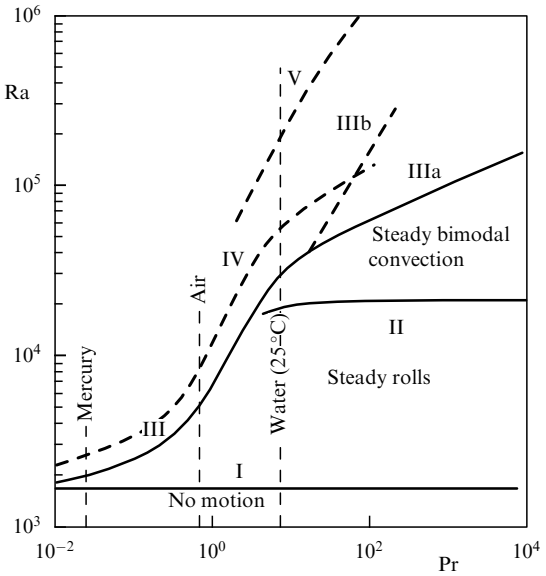

Figure 5. Diagram of convection regimes in the plane of the Rayleigh number $\mathrm{Ra} = \rho_0 \alpha g V \Delta T/(\rho_1 \nu \varkappa)$ vs the Prandtl number $\mathrm{Pr} = \nu/\varkappa$. Here, ρ_0 is the initial fluid density (at a temperature T_1), ρ_1 is its final density (at a temperature T_2), α is the isobaric-thermal-expansion coefficient, g is the free-fall acceleration, $\Delta T = T_2 - T_1$, V is a selected unit volume of fluid, $\varkappa$ is the thermal diffusivity, $\varkappa = \mu c_p/\lambda$, μ is the dynamic viscosity, c_p is the specific heat at constant pressure, λ is the thermal conductivity, and $\nu = \mu/\rho$ is the kinematic viscosity.

As a result, a complex pattern develops on the water surface [14 – 19].

Figure 5 presents a diagram of convection regimes in the (Rayleigh number) – (Prandtl number) coordinates, which summarizes experimental data obtained by several investigators [20 – 23]. Below line I ($\mathrm{Ra} = \mathrm{Ra_c}$), the region of the stable state of the fluid is located and above this line, the region of steady roll convection. Curve II is the threshold above which the cross-roll instability gives rise to bimodal convection. The splitting of curve III into two branches reflects the fact that the shape of the structures becomes strongly dependent on the prehistory of the flow (i.e., on random nonuniformities). The nonuniformities can give rise to oscillations of some fluid volumes (curve IIIa). If we try to remove the nonuniformities, the steady pattern may exist at higher Ra (up to branch IIIb). Curve IV corresponds to the excitation of higher harmonics in the spectrum of oscillations associated with changes in the heat flux. Above curve V, the region of fully turbulent convection is located [10].

However, in any fluid, including water, the set of convection structures is richer than that represented in the diagram in Fig. 5. An exact diagram of all structures that can develop in fluids cannot be constructed. Their diversity depends not only on the transitions between different forms of convection but also on the shape and depth of the container, on the material of its walls (viz., on their wettability), on the initial conditions for the development of convection, etc. In real fluids, not only cells and rolls can be observed but, as we show in Section 4, also prominences and spiral patterns can develop. A fairly detailed description of basic transitions between various convection regimes can be found in Ref. [24].

As water evaporates from a surface, the driving force of vertical convection is basically concentrated in the middle layers of water, where the temperature is at a maximum (see Fig. 4). However, the motion-triggering mechanism is related to the fluid surface and is controlled by the decrease in its temperature due to the evaporation of water. Because of evaporation, the surface is always colder than the bulk of the fluid. It is interesting that the presence of a vertical temperature gradient is a necessary but not a sufficient condition for the onset of large-scale convection. The magnitude of this gradient is important. For the emergence of an Archimedean force and the initiation of vertical motion, the following condition must necessarily be satisfied: *thermal variations at the surface should not have time to dissipate due to thermal conduction before they give rise to vertical displacements of the fluid*. Likely, Rayleigh was aware of this fact [25, 26].

Thus, there are two characteristic times — the displacement time τ_d and the thermal-relaxation time τ_r. The former is inversely proportional to the isobaric thermal expansion coefficient and the latter is inversely proportional to the thermal diffusivity (thermal conductivity) of the fluid. The condition for the onset of motion is $\tau_\mathrm{r} > \tau_\mathrm{d}$ [27 – 29].

The formation of macroscopic structures in water due to its convection is a good illustration for the self-organization mechanism associated with chaos $\leftrightarrow$ order transitions that occur if temperature gradients are present [30, 31]. The motion of the water molecules affected by the thermal gradients then becomes collective (directional), rather than random. We recall that cellular patterns (Bénard cells) present the most prominent example of self-organization. In his study [11], which became a classic, Bénard observed cells that developed in a layer of sperm-whale oil heated from below (these cells later came to be known as Bénard cells).

Although the cellular pattern is maintained by vertical displacements of the fluid, it is produced not only by Rayleigh convection. The notion of 'thin layer' is crucial for this process [32]. Marangoni was the first to note this fact. He observed the development of cells in the layer of a liquid paint during the coloration of a sufficiently hot surface. These cells emerge even if the painted sheet is positioned vertically, such that no convection (no Archimedean force) is present. Cells develop on vertical sheets due to the *thermocapillary effect* related to variations in the surface tension of the fluid, if the condition $\mathrm{Ma} > 1$ is satisfied; here,

$$\mathrm{Ma} = \frac{\Delta\sigma}{\rho \nu \varkappa}\, r$$

is the Marangoni number, where $\Delta\sigma$ is the variation in the surface-tension coefficient over the fluid surface, r is the radius of the cell that develops on the surface, ρ is the density, ν is the kinematic viscosity, and $\varkappa$ is the thermal diffusivity.

Thus, two conditions must be satisfied simultaneously for the emergence of a cellular pattern. The first condition is the presence of a gradient, or two spatially separated regions — one heated and one cold; this ensures vertical displacements of the fluid and specifies the vector of their direction. The second necessary condition is the interaction between the modes that are excited in the process of motion. As they compete, one spatiotemporal mode survives, stabilizes, and manifests itself as a stable cellular pattern [10, 30].

If the thermal gradients are small, the structures that develop on the fluid surface in the process of natural evaporation (without heating) can hardly be seen by the naked eye. They can be observed using an IR imager.

4. Spiral water-convection macrostructures

In the Rayleigh – Bénard convection, either spiral patterns or circular, funnel-type structures can be observed under certain conditions together with the cells. They were discovered more than ten years ago [36].

Such patterns were observed in liquid sulphur hexafluoride, SF_6, with the density $\rho_c = 0.73$ g cm^{-3}, at the temperature $T = 45.7\,^\circ$C and the pressure $P = 37.8$ bar, in a container of diameter 102 cm and depth 19 cm. Spiral patterns can be observed at Pr < 3.5, while structures in the form of circular funnels (Figs 6a, 6c) develop at Pr > 3.5, up to Pr $= 30$. It is interesting that visually similar patterns can be observed in a thin water layer where the oscillatory Belousov – Zhabotinsky reaction occurs (Figs 6b, 6d).

Assenheimer and Steinberg [36] mention this reaction. However, such patterns in the Belousov – Zhabotinsky reaction develop due to a different mechanism, related not to the Rayleigh – Bénard convection but to autowave processes in the thin fluid layer, as the result of the oscillatory reaction of malonic-acid-analogs oxidation by bromate with the presence of variable-valence metals — cerium or iron — as catalysts. We studied this process more than 20 years ago [33 – 35]. Various autowave processes and their mathematical models were considered in review article [37] published in *Physics – Uspekhi*.

Recently, with the use of IR imaging, we managed to observe spiral patterns that developed during the cooling of water in a rectangular, 35 × 24 cm plastic container of depth 2.5 cm. If water heated to $T = 36.6\,^\circ$C – $40\,^\circ$C is poured into such a motionless container, a spiral pattern appears. Two spirals wound in opposite directions were observed. The development of such a structure is due to the Rayleigh – Bénard convection. These structures appear at atmospheric pressure in the temperature range from $36.6\,^\circ$C to $34.8\,^\circ$C at Pr < 6.5 and room temperature $21.5\,^\circ$C. The presence of these structures can be observed over three minutes. Figure 7 shows a sequence of IR (8 – 12 μm) images representing this process. At a first glance, the initial pattern shown in Fig. 7 appears to be produced by an artificially created fluid stream directed from one edge of the container to the other. However, this is not the case. The formation of spirals is controlled by convection processes, although we cannot completely exclude the possibility that it is stimulated by initial conditions, i.e., the very process of pouring water into the rectangular container.

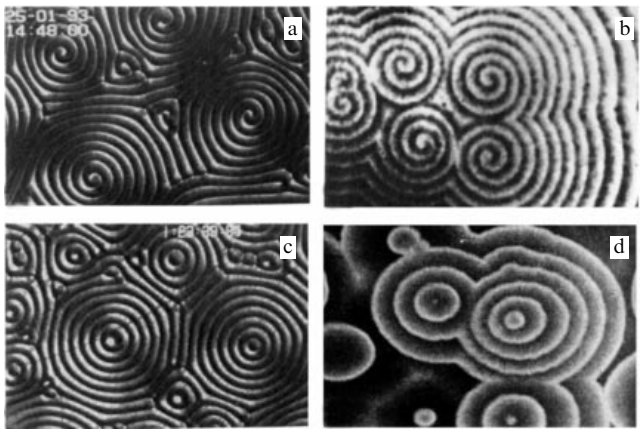

Figure 6. Two types of similar convection patterns: (a) spiral waves in liquid sulphur hexafluoride, SF_6 [36]; (b) spiral waves in the Belousov – Zhabotinsky reaction [34]; (c) circular target-type structures in liquid sulphur hexafluoride, SF_6 [36]; (d) circular target-type structures in the Belousov – Zhabotinsky reaction [34].

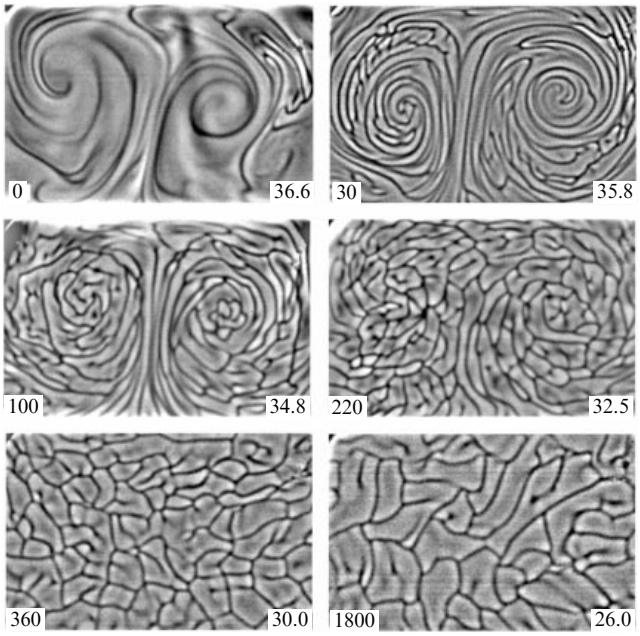

Figure 7. Sequence of images showing the pattern evolution during the transient water-cooling process in a rectangular container of sizes 35 × 24 × 2 cm, as observed in the 8 – 12 μm IR range. The temperature varied from $36.6\,^\circ$C to $26\,^\circ$C. The time in seconds is indicated at the lower left corner of each frame and the temperature of the water in degrees centigrade at the lower right corner. The room temperature was $21.5\,^\circ$C.

As the water cools, the spiral structures gradually disintegrate into separate cells. Nine minutes later, when the temperature of the water reaches $29\,^\circ$C, the water pattern becomes cellular and free of spiral features. Further changes in these cellular structures are slow. Even if the mean temperature of the water is equal to that of the ambient medium, the evaporation from the surface of the container produces a bulk temperature gradient, and therefore convection persists and the cellular pattern is maintained. This pattern disappears only if the evaporation is terminated, for instance, if the container is covered with a lid.

It is known that the appearance of the pattern depends not only on the physical properties of the fluid and the position of the heating point but also on the shape of the container [38]. Figure 8 shows a sequence of images of the pattern developing in the cooling water that, in contrast to the situation shown in Fig. 7, was poured into a motionless circular container of diameter 17 cm. Other parameters are the same as in the case illustrated by Fig. 7. Spiral macroscopic vortices are not observed in the circular plastic container, but numerous microscopic funnel vortices are present at the same temperatures; they can be seen as black dots in Fig. 8. As the water cools, the microscopic funnel vortices gradually disappear and the entire pattern disintegrates into individual, irregularly shaped cells. The cellular patterns present in the water that has already cooled exhibit virtually no differences between the cases of the rectangular and circular containers.

The possibility of pattern formation in water also depends on the depth of the fluid layer. The dependence of this process on the depth can easily be revealed in a simple experiment

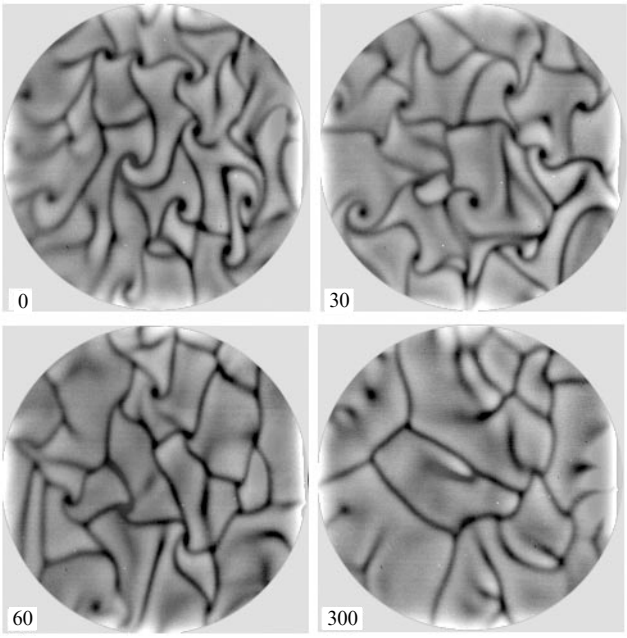

Figure 8. Sequence of images showing the pattern evolution during the transient water-cooling process in a circular container of diameter 17 cm, as observed in the 8 – 12 μm IR range. The temperature varied from 40 °C to 20 °C. The time in seconds is indicated at the lower left corner of each frame. The room temperature was 21.5 °C.

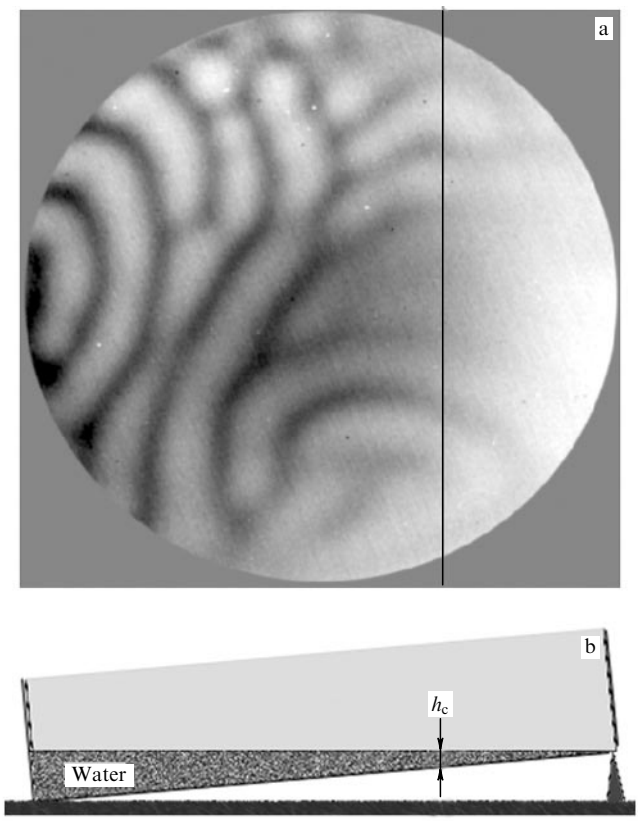

Figure 9. (a) Structures occurring in an inclined container. (b) Measuring the thickness h of the water layer by inclining the container; h_c is the critical layer thickness at which structure formation is stopped. The container diameter is 17 cm. In the bottom left corner, the water layer thickness is 10 mm, with $h_c = 0.2$ mm .

(Fig. 9). The oscillation periods of the surface layer and of the low-frequency vertical convection are proportional to h^2, where h is the depth of the fluid layer. If the container is inclined, Rayleigh – Bénard cells disappear in the region where $h < h_c$.

5. Mobility of a perfluorodecaline drop on the water surface

It is known that observing the motion of drops of various fluids over the water surface permits studying the physical – chemical properties of water itself and of the substances that form the drops [39 – 43]. We used drops of perfluorodecaline. The interest of biophysicists in perfluorocarbonic compounds stems from their high gas-dissolving power; for this reason, they are widely employed in the development of various medical preparations (gas-transporting blood substitutes, membrane-modifying agents, wound coverings, etc.).

Perfluorodecaline is not a polar compound. It is similar to naphthalene in its structure; however, it has all hydrogen molecules substituted with fluorine ($C_{10}F_{18}$). This compound is a liquid perfluorocarbon, and therefore chemical inertness and water-insolubility are characteristic of it, as of all other perfluorocarbons [44, 45]. In their surface charge, perfluorocarbon molecules are virtually neutral. Therefore, intermolecular electric interactions are inappreciably weak in liquid perfluorocarbons. In essence, perfluorocarbonic liquids are similar to gases in their properties. This accounts for their extremely weak surface tension, below 20 dyn cm^{-1} (whereas the surface tension of water is of the order of 70 dyn cm^{-1}), and high gas-dissolving power (the volumetric solubility is up to 50 vol. % for O_2 and up to 200 vol. % for CO_2).

It was recently found that the four-component, water – lipid – perfluorocarbon – air system demonstrates an unusual physical phenomenon, spontaneous lipid mobility [39, 41 – 43]. We considered the mechanism of this phenomenon, which results from the differences in the volumetric expansion between these three substances, variations in their surface tension, and their evaporation. It should be noted that a similar study was published last year by a Japanese research group headed by Yutaka Sumino, Kyoto [46]. The authors of Ref. [46] constructed a system that included the solution of a surfactant (trimethylammonium chloride and nitrobenzene with sodium iodide) in which a drop of oil demonstrated oscillatory spatial displacements under certain boundary conditions. Evidently, other variants of similar systems including four or more components are possible. We do not consider the description of multicomponent systems of this sort, because IR imaging was not employed in investigating them. The reader can become acquainted with some of them using literary sources, e.g., a review published in *Physics – Uspekhi* [43].

We restrict ourselves to only one example of using IR imaging. We have recently shown that the spontaneous mobility of a drop arises even in a three-component system, perfluorodecaline drop – water surface – air [41]. We carried out the following experiment. A Petri dish of diameter 9 cm was filled with distilled water to a height of approximately 5 mm at a temperature of about 24 °C. A perfluorodecaline drop of volume 2 μl was placed on the water surface (Fig. 10a).

Perfluorodecaline is almost twice as heavy as water; nevertheless, the drop does not sink and remains on the water surface. The retention of the drop on the water surface

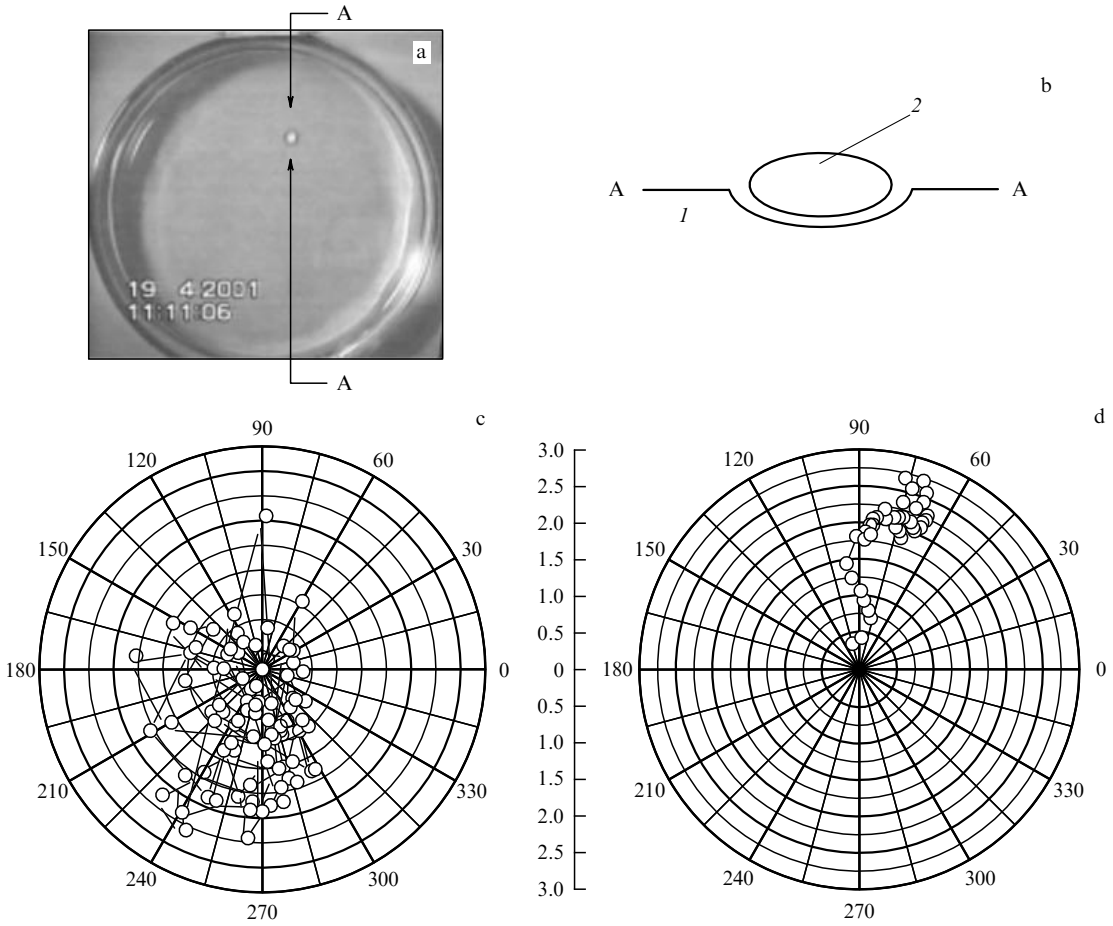

Figure 10. Motion of the perfluorodecaline drop over the water surface: (a) a photograph of the drop in the Petri dish (of diameter 9 cm); (b) schematized cross section of the drop along the AA line (see Fig. 10a): *1*, water; *2*, perfluorodecaline drop; (c) trajectory of the fast motion of the drop; (d) trajectory of the slow motion of the drop (the initial position of the drop is at the coordinate origin). The time interval between recordings of the position of the drop on the water surface is 3 s.

is favored by the hydrophobic properties of the surface of the drop. The solubility of perfluorodecaline in water is very low (3×10^{-6} vol %). Another factor that favors the retention of the drop is the high surface tension of water. The force supporting the drop is due to a depression of the water surface produced by the weight of the overlying drop. A schematic of the drop placed on the water surface is shown in Fig. 10b.

Our observations of the behavior of the perfluorodecaline drop revealed two motion regimes of the drop — first, spontaneous, relatively fast, stochastic motion similar to Brownian motion at first glance and, second, a slow drift without pronounced trajectory breaks.

The trajectories of the drop in the fast and slow motion regimes are shown in Figs 10c, 10d. If the drop moves rapidly, 1 – 4 cm-long rectilinear paths alternate with random changes in the direction of motion; the speed in this case is 0.75 – 1 mm s^{-1}. In the case of slow movement, the speed does not exceed 0.1 mm s^{-1}, being thus an order of magnitude lower (Fig. 10d). A perfluorodecaline drop of volume 2 μl has the mass 4 mg, i.e., it is too heavy for its mobility to be accountable for by random impacts of water molecules (as Brownian motion is usually explained).

Our experiments indicated that the motion of the drop is induced by impacts of air bubbles dissolved in water. If distilled water is poured into a Petri dish and then allowed to settle over a day in the open dish, its air content is reduced, and it comes into gas balance with the ambient medium. In this case, the content of dissolved air gases is less than 2 vol % (at $T = 24\,^{\circ}\mathrm{C}$). If a perfluorodecaline drop is placed on the surface of such water, the drop either drifts slowly or remains virtually motionless. But if the drop is placed on the surface of water freshly poured into a Petri dish, which has absorbed air during the jet pouring, the drop starts actively moving.

The surface tension of water is 3 – 4 times higher than that of perfluorocarbons. These particular properties of perfluorocarbons dictate the character of their interaction with both water and microbubbles of air emanating from the water. The 'billiards model' that is frequently used to explain the mechanism of Brownian motion is not applicable in this case. The interaction of microbubbles of gas dissolved in the water with the perfluorocarbon drop is not the energy transfer due to collisions of elastic spheres but rather the interaction of two fluids, which have different surface tensions and gas solubilities, at their interface.

Each microbubble emerging from the water and contacting the perfluorocarbon drop has a kinetic energy, which is very small, however. Simple calculations [41] show that the kinetic energy of an air microbubble of size 0.5 mm is of the order of 10^{11} erg. This energy is insufficient to set a perfluorocarbon drop of mass 4 mg in motion. The main energy source is not the impact kinetic energy but the energy

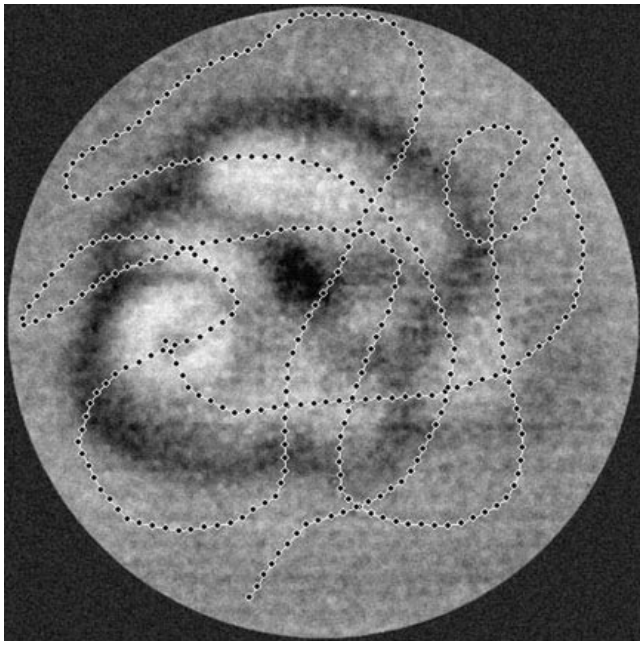

Figure 11. Trajectories of drop motion and heated spots formed in water during the movement of a perfluorodecaline drop, as observed in the 8 – 12 μm IR range.

associated with the destruction of the microbubble interacting with the drop. The microbubble breaks down as it contacts the drop; the air comes from the bubble into the perfluorocarbon drop. It is this process that provides the main energy source. For a microbubble of size 0.5 mm, the energy released in this process is around 1 erg. Thus, the mobility of the drop is basically due to the destruction of microbubbles.

Observations of drop motion by an IR imager have revealed another particular feature. The moving drop leaves a trail of heated water behind itself. The formation of the light trail was observed only in the case of fast motion of the drop (Fig. 11), i.e., when the drop was gas-saturated [47]. If the water did not contain a gas, and the perfluorodecaline drop did not move, only a dark, virtually motionless spot of cold water was observed.

The formation of the thermal trail behind the drop results from the thermal nonuniformity of the drop in the vertical direction: the evaporation of perfluorodecaline makes the upper part of the drop colder than its lower part, which interacts with air bubbles. In the process of heating, part of the perfluorodecaline drop passes onto the water surface and covers it with a molecular film, which impedes evaporation. As this takes place, the surface temperature of the water in the neighborhood of the drop increases. Because of the relatively low heat conductivity of water, the thermal trail persists for some time; the resulting thermal relief on the water surface, in turn, restricts the stochastic motion of the drop. Therefore, *such a system is self-organizing, and the drop interacting with water restricts by itself the number of the degrees of freedom for its motion.*

6. Conclusion

Several dozen various (chemical, biochemical, and biological) methods of monitoring the purity of water are currently in use [48]. As regards the practical applications of IR imaging to observations of convection patterns in water, the results of further studies of such patterns could be applied to the techniques of proximate control of quality and state of water in basins. Adding various impurities to water (such as surfactants, organic compounds, salts, and acids) changes the surface tension of water at the water – air interface. All such admixtures result in specific changes in the structure of Rayleigh – Bénard cells. It is plausible that the above-described procedure of IR recording of water structures could be used in developing techniques for the proximate monitoring of water pollution, because the evolving structures reflect not only the shape of the container and the material of its walls but also the impurities present in the water. It should be recalled in this context that, on the initiative of the UN, the year 2003 was declared *the International Year of Freshwater* [49, 50].

As concerns IR imaging in general, it is now reasonable to expect that it will become one of the most important information technologies, with an extensive area of application. In biology, it could be used to investigate the heat production of living organisms and individual organs depending on diurnal and seasonal cycles. In medicine, the field of application of IR imaging could encompass the diagnostics of vascular, inflammatory, and tumorous diseases, checking the efficiency of treatment, and proximate control in quarantine measures. The IR-imaging equipment permits carrying out the fire-preventive monitoring of forest tracts and peat beds and keeping track of volcanic activities, the movement of permafrost, steppe, and desert zones, and the migration of animals. In technology, IR imagers make it possible to check the operation of machines and mechanisms, the functioning of power-transporting networks, and the preservation of the thermal insulation of buildings and structures.

Our study was done in the framework of the research program *Basic science for medicine* of the Russian Academy of Sciences for 2003 – 2005 (section *Development and improvement of diagnostic techniques*); however, it elucidated the potential of IR imaging in resolving a variety of tasks raised not only by medicine but also by diverse branches of physics.

Acknowledgments. We are grateful to A B Medvinskii and G N Sarkisov for discussions and to the referees for valuable remarks.

References

1. Gaussorgues G *La Thermographie Infrarouge*: *Principes, Technologies, Applications* (Paris: Lavoisier, 1984) [Translated into English: *Infrared Thermography* (London: Chapman&Hall, 1994); translated into Russian (Moscow: Mir, 1988)]
2. Kovalev A V, Fedchishin V G, Shcherbakov M I *Spetsial'naya Tekh.* (3) 13; (4) 19 (1999)
3. Pevtsov E, Chernokozhin V *Elektronnye Komponenty* (1) 32; (2) 30; (3) 12 (2001)
4. Breen T B et al. *Proc. SPIE* **3436** 530 (1998)
5. Pengelley R, Hewish M "In the heat of the night" *Jane's Int. Defense Rev.* **34** (10) 49 (2001)
6. Ivanitskii G R *Vestn. Ross. Akad. Nauk* **76** (2006) (in press)
7. Ivanitsky G R et al. *Dokl. Ross. Akad. Nauk* **393** 419 (2003) [*Dokl. Biol. Sci.* **393** 496 (2003)]
8. Ivanitskii G R et al. "Issledovanie mikrotsirkulyatsii krovi s pomoshch'yu sovremennykh metodov termografii pri vvedenii perftorana" ("Investigation of blood microcirculation using modern thermographic techniques with perfluorane introduction"), in *Perftoruglerodnye Soedineniya v Meditsine i Biologii* (Perfluorocarbonic Compounds in Medicine and Biology) (Eds G R Ivanitskii, E B Zhiburt, E I Maevskii) (Pushchino, 2004) p. 10

9. Ivanitskii G R *Dokl. Ross. Akad. Nauk* **398** 709 (2004) [*Dokl. Biol. Sci.* **398** 367 (2004)]
10. Getling A V *Usp. Fiz. Nauk* **161** (9) 1 (1991) [*Sov. Phys. Usp.* **34** 737 (1991)]
11. Bénard H *Rev. Gén. Sci. Pures Appl.* **11** 1261, 1309 (1900)
12. Gollub J P, McCarriar A R, Steinman J F *J. Fluid Mech.* **125** 259 (1982)
13. Wesfreid J E, Zaleski S (Eds) *Cellular Structures in Instabilities* (Berlin: Springer-Verlag, 1984) p. 33
14. Cui Q, Smith V H (Jr) *J. Chem. Phys.* **113** 10240 (2000)
15. Mishima O, Stanley H E *Nature* **396** 329 (1998)
16. Montrose C J et al. *J. Chem. Phys.* **60** 5025 (1974)
17. Busse F H *J. Fluid Mech.* **52** 97 (1972)
18. Clever R M, Busse F H *J. Fluid Mech.* **65** 625 (1974)
19. Busse F H *Rep. Prog. Phys.* **41** 1929 (1978)
20. Busse F H, Clever R M *J. Fluid Mech.* **102** 75 (1981)
21. Krishnamurti R *J. Fluid Mech.* **42** 295 (1970)
22. Krishnamurti R *J. Fluid Mech.* **60** 285 (1973)
23. Busse F H, in *Hydrodynamic Instabilities and the Transition to Turbulence* (Eds H L Swinnery, J P Gollub) (Berlin: Springer-Verlag, 1981) [Translated into Russian (Moscow: Mir, 1984) p. 124]
24. Getling A V *Konvektsiya Releya – Benara. Struktura i dinamika* (Rayleigh – Bénard Convection: Structures and Dynamics) (Moscow: Editorial URSS, 1999) [Translated into English (Singapore: World Scientific, 1998)]
25. Rayleigh, Lord *Philos. Mag.* **32** 529 (1916)
26. Rayleigh, Lord *Proc. R. Soc. London, Ser. A* **93** 148 (1916)
27. Gollub J P, McCarriar A R, Steinman J F *J. Fluid Mech.* **125** 259 (1982)
28. Heutmaker M S, Gollub J P *Phys. Rev. A* **35** 242 (1987)
29. Ahlers G, Cannell D S, Steinberg V *Phys. Rev. Lett.* **54** 1373 (1985)
30. Haken H *Synergetics* (Berlin: Springer-Verlag, 1978) [Translated into Russian (Moscow: Mir, 1980)]
31. Ivanitskii G R, Krinskii V I, Sel'kov E E *Matematicheskaya Biofizika Kletki* (Mathematical Cell Biophysics) (Moscow: Nauka, 1978)
32. Edel'man E D *Sorosovskii Obraz. Zh.* **6** (5) 94 (2000)
33. Zaikin A N, Zhabotinsky A M *Nature* **225** 535 (1964)
34. Ivanitsky G R et al. *Biol. Rev. Sec. D* **2** 279 (1981)
35. Krinskii V I, Mikhailov A S *Avtovolhy* (Autowaves) (Moscow: Znanie, 1984) p. 28
36. Assenheimer M, Steinberg V *Nature* **367** 345 (1994)
37. Ivanitskiĭ G R, Medvinskiĭ A B, Tsyganov M A *Usp. Fiz. Nauk* **164** 1041 (1994) [*Phys. Usp.* **37** 961 (1994)]
38. Somerscales E F C, Dougherty T S *J. Fluid Mech.* **42** 755 (1970)
39. Ivanitskii G R et al. *Dokl. Ross. Akad. Nauk* **374** 548 (2000) [*Dokl. Biophys.* **373/375** 41 (2000)]
40. Ivanitskii G R et al. *Dokl. Ross. Akad. Nauk* **375** 685 (2000) [*Dokl. Biophys.* **373/375** 56 (2000)]
41. Ivanitsky G R, Kravchenko V V, Tsyganov M A *Dokl. Ross. Akad. Nauk* **383** 263 (2002) [*Dokl. Biochem. Biophys.* **383** 88 (2002)]
42. Stoilov Yu Yu *Langmuir* **14** 5685 (1998)
43. Stoĭlov Yu Yu *Usp. Fiz. Nauk* **170** 41 (2000) [*Phys. Usp.* **43** 39 (2000)]
44. Matsuo M, Otosi S *Soedineniya Ftora* (Fluorine Compounds) (Moscow: Mir, 1990)]
45. Simons J H (Ed.) *Fluorin Chemistry* (New York: Academic Press, 1964)
46. Sumino Y et al. *Phys. Rev. Lett.* **94** 068301 (2005)
47. Ivanitskii G R et al. "Termograficheskoe issledovanie dinamiki dissipativnykh struktur v sisteme iz nesmeshivaemykh zhidkostei" ("Thermographic investigation of the dynamics of dissipative structures in a system of immiscible fluids"), in *Gorizonty Biofiziki: ot Teorii k Praktike* (Horizons for Biophysics: from Theory to Practice) (Ed. G R Ivanitskii) (Pushchino, 2003) p. 52
48. Ostrovskii V M et al. *Voda: Indikatornye Sistemy* (Water: Indicating Systems) (Moscow: VINITI, 2002)
49. Smirnova M *V Mire Nauki* (11) 24 (2003)
50. Potapova T *V Mire Nauki* (11) 78 (2003)